Dynamics of a Self-Propelled Particle in a Harmonic Trap

Olivier Dauchot[1] and Vincent Démery[1,2]
[1]Gulliver, UMR CNRS 7083, ESPCI Paris, PSL Research University, 10 rue Vauquelin, 75005 Paris, France
[2]Univ Lyon, ENS de Lyon, Univ Claude Bernard Lyon 1, CNRS, Laboratoire de Physique, F-69342 Lyon, France

(Received 31 October 2018; published 13 February 2019)

The dynamics of an active walker in a harmonic potential is studied experimentally, numerically, and theoretically. At odds with usual models of self-propelled particles, we identify *two* dynamical states for which the particle condensates at a finite distance from the trap center. In the first state, also found in other systems, the particle points radially outward from the trap, while diffusing along the azimuthal direction. In the second state, the particle performs circular orbits around the center of the trap. We show that self-alignment, taking the form of a torque coupling the particle orientation and velocity, is responsible for the emergence of this second dynamical state. The transition between the two states is controlled by the persistence of the particle orientation. At low inertia, the transition is continuous. For large inertia, the transition is discontinuous and a coexistence regime with intermittent dynamics develops. The two states survive in the overdamped limit or when the particle is confined by a curved hard wall.

DOI: 10.1103/PhysRevLett.122.068002

Understanding the effect of confinement on active systems has become a central topic of research in active matter. The motivation is twofold. On one hand, living organisms and self-propelled particles rarely evolve in an unbounded medium [1]; understanding their behavior in confined environments is key to understanding realistic systems. On the other hand, confining self-propelled particles within an external trap is an excellent means of analyzing the dynamics and the mechanical pressure developed by such systems [2–8].

The mean square displacement of an isolated particle is the same for the three main models of self-propelled particles introduced so far, namely, active Brownian particles (ABPs), run-and-tumble particles, and active Ornstein-Uhlenbeck particles [9,10]. It is thus not a discriminating observable. The steady state density profile in a confining potential is far more informative, and has recently received considerable attention [4,11]. Apart from the notable exceptions of run-and-tumble particles in one dimension and active Ornstein-Uhlenbeck particles in a harmonic trap, the exact steady state is unknown. However, theoretical approximations, numerical simulations [4,11,12], and experiments with colloids in an acoustic trap [6] show that self-propelled particles confined in a 2D axisymmetric trap accumulate at a finite distance of the trap center when the trap is stiff. The reason is that the self-propelled particle climbs the potential until it gets stuck with its orientation pointing radially outward of the trap, at a distance shorter than the persistence length of its isolated dynamics.

This is however in sharp contrast with the simplest experiment one can think of: observing a hexbug nano [13] in a parabolic antenna. As can be seen from Fig. 1, and from movie 1 provided in the Supplemental Material [14], the hexbug orbits around the trap center. The goal of this Letter is to examine the reasons for such a discrepancy. Possible factors are inertia, which until recently [15] has been overlooked in the active matter literature, and self-alignment [16,17], which is responsible for the collective motion of isotropic walkers [18]. We show that this self-alignment is the key ingredient for observing rotating orbits. Furthermore, we demonstrate that there is a transition from the "orbiting" state to the "climbing" state depending on the persistence time of the particle orientation. Finally, the nature of the transition is controlled by inertia. For large relaxation time of the velocity, the transition is discontinuous and an intermittent dynamics between the two states is observed. For small relaxation time, the transition is continuous. Remarkably, the transition subsists in the overdamped limit.

The experimental setup is composed of one hexbug, a toy robot [13], confined within a parabolic dish (Fig. 1).

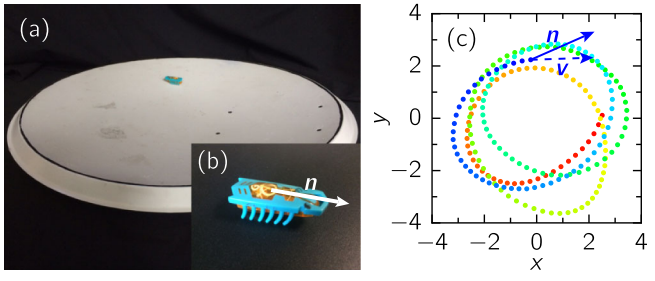

FIG. 1. Hexbug nano [19] (b) running in a parabolic dish (a). (c) Observed orbiting trajectory, the arrows represent the particle orientation $\boldsymbol{n}$ and velocity $\boldsymbol{v}$; see also movie 1 in Supplemental Material [14].

The parabola (Grundig QGP 2400) has an elliptic section with a small axis of 580 mm, a long axis of 630 mm, and is 50 mm deep. The hexbug motion is tracked at 25 Hz using a standard CCD camera. The hexbug has a length $L = 45$ mm, a width 15 mm, a height 15 mm, and a mass $m = 7.5$ g, including the battery. Its motion is obtained from an internal vibration (frequency $f_0 = 115$ Hz and acceleration $\Gamma_0 \simeq 1.5g$) transmitted to 12 legs whose shape ensures propulsion at a speed $v_0 \simeq 100$ mm/s. The persistence length of the motion exceeds 1 m. Another way to set the hexbug in motion is to shake it vertically at the same frequency f_0, while keeping the engine off. The parabola is thus attached to a vibrating shaker, which provides a sinusoidal motion with an acceleration $\Gamma \in [1-3]g$. Note that the vibration amplitude not only ensures the deterministic motion of the hexbug, but also contributes to the stochastic part of it. In the following we choose L as the unit length, while the time is expressed in seconds.

Our main experimental finding is that there is a transition from an orbiting motion to a climbing motion when, the vibration being on, the propulsive power of the hexbug decreases as the battery gets low (see movie 2 in Supplemental Material [14]). Figure 2 illustrates the two regimes obtained in "steady state" conditions: (i) engine on with a new battery and (ii) engine off with a low level of vibration. In the orbiting regime, the hexbug rotates around the bottom of the parabola, sometimes reverting its orbiting direction. The radial position fluctuates significantly. The velocity $\boldsymbol{v}$ and the orientation of the hexbug longitudinal axis $\boldsymbol{n}$ are closely aligned ($(\boldsymbol{v}/\|\boldsymbol{v}\|)\cdot\boldsymbol{n} > 0.8$). In the climbing regime, the hexbug orientation points radially away from the center of the parabola. The motion is localized on a well-defined radial position. The azimuthal velocity fluctuates around zero and the angular motion is diffusive. The transition is essentially independent from the vibration amplitude as long as $\Gamma > 1.5g$. The same transition is observed when the hexbug engine is switched off and the vibration amplitude Γ is increased from $1g$ to $2g$. The precise location of the transition is hard to determine, the reason being that there is a range of vibration for which there is a coexistence of the two dynamics, leading to intermittent motion.

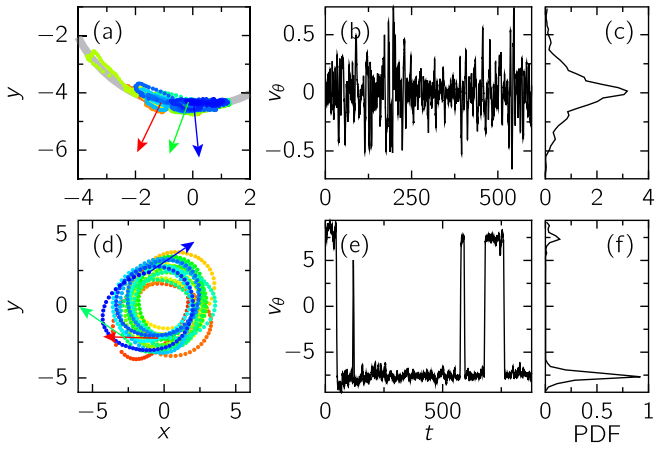

FIG. 2. Experimental dynamical regimes. (a)–(c) Climbing motion. The hexbug is stuck, facing the slope, at a given height in the potential and diffuses laterally; engine on, $\Gamma = 1.8g$. (d)–(f) Orbiting motion. The hexbug rotates around the center of the parabola; engine off, $\Gamma = 1.0g$. (a), (d) Trajectory. The color codes the time; the orientation of the hexbug body is shown with arrows at three different times. (b), (e): Azimuthal velocity as a function of time. (c), (f). Probability distribution (PDF) of the azimuthal velocity.

To better examine this transition and identify the proper control parameters, we adopt a description of the self-propelled particle inspired from the one introduced to describe granular walkers [16]: the velocity $\boldsymbol{v}$ and orientation $\boldsymbol{n}$ obey

$$m\dot{\boldsymbol{v}} = F_0\boldsymbol{n} - \gamma\boldsymbol{v} - \kappa\boldsymbol{r}, \tag{1}$$

$$\tau\dot{\boldsymbol{n}} = \zeta(\boldsymbol{n}\times\boldsymbol{v})\times\boldsymbol{n} + \sqrt{2\alpha}\xi\boldsymbol{n}_\perp. \tag{2}$$

Equation (1) contains the mass of the hexbug m, the self-propulsive force F_0, the friction coefficient γ, and the stiffness κ of the harmonic potential; in the absence of confinement, the hexbug moves with a velocity $v_0 = F_0/\gamma$. The orientation dynamics [Eq. (2)] is overdamped and contains the key ingredient, specific to the model, namely, a self-aligning torque of the orientation $\boldsymbol{n}$ towards the velocity $\boldsymbol{v}$. This torque originates from the fact that the dissipative force is not symmetric with respect to the propulsion direction $\boldsymbol{n}$ when $\boldsymbol{v}$ is not aligned with $\boldsymbol{n}$. This ingredient is at the root of the emergence of collective motion in a system of vibrated polar disks [16,20]. Finally, the orientation dynamics contains a Gaussian noise $\xi(t)$ with correlations $\langle\xi(t)\xi(t')\rangle = \delta(t-t')$; α/τ^2 is the rotational diffusion coefficient.

Rescaling the length by $r_0 = F_0/\kappa$ and the time by $t_0 = \gamma/\kappa$, we arrive at the dimensionless equations of motion,

$$\tau_v\dot{\boldsymbol{v}} = \boldsymbol{n} - \boldsymbol{v} - \boldsymbol{r}, \tag{3}$$

$$\tau_n\dot{\boldsymbol{n}} = (\boldsymbol{n}\times\boldsymbol{v})\times\boldsymbol{n} + \sqrt{2D}\xi\boldsymbol{n}_\perp, \tag{4}$$

which contain three parameters, $\tau_v = m\kappa/\gamma^2$, $\tau_n = \tau\kappa/(\zeta F_0)$, and $D = \alpha\gamma\kappa/(\zeta F_0)^2$. Note that τ_v does not depend on F_0, while τ_n increases when F_0 decreases.

We simulate Eqs. (3) and (4) with a small noise amplitude $D = 0.01$ and recover the behavior observed in the experiments: for different values of τ_n and τ_v, the particle adopts either a climbing [$\tau_v = 0.2$, $\tau_n = 1.5$, Figs. 3(a)–3(f)] or an orbiting dynamics [$\tau_v = 0.2$, $\tau_n = 0.5$, Figs. 3(g)–3(l)]. In both cases the particle is localized at a finite distance from the center of the parabola, but the distribution is sharply peaked at $r = 1$ in the climbing state, while it is more

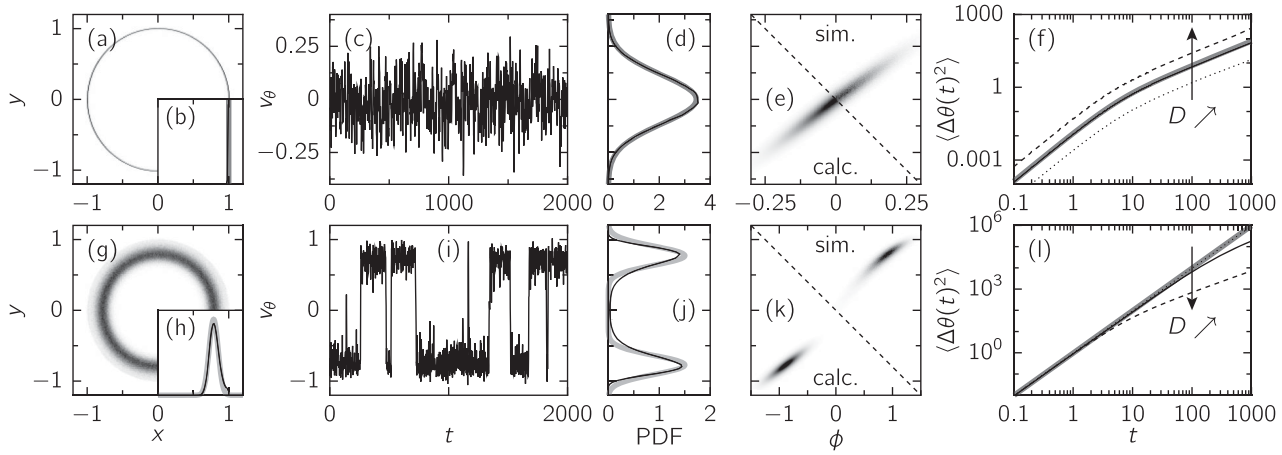

FIG. 3. Numerical dynamical regimes. Simulations for $\tau_v = 0.2$, $D = 0.01$, and (a)–(f) climbing dynamics $\tau_n = 1.5$, (g)–(l) orbiting dynamics, $\tau_n = 0.5$. (a),(g) (x, y) probability density function (PDF). (b), (h) PDF of the distance to the parabola center, (c), (i) Azimuthal velocity as a function of time. (d), (j) PDF of the azimuthal velocity (thin black lines) and theoretical prediction at weak noise (thick gray lines). (e), (k) PDF in the orientation-azimuthal velocity plane from simulations (top right) and weak noise calculation (bottom left). (f), (l) mean squared angular displacement (MSAD) of the angular coordinate θ (thin solid line) and theoretical prediction (thick gray line). Dotted and dashed lines: MSAD for $D = 0.002$ and $D = 0.05$, respectively.

broadly distributed in the orbiting state [Figs. 3(b) and 3(h)]. In the climbing state, the azimuthal velocity fluctuates around 0, while, in the orbiting state, it fluctuates around two opposite finite values, and the sign changes corresponding to spontaneous inversions of the rotation direction [Figs. 3(c), 3(d), 3(i), and 3(j)]. In both cases, the direction of motion is directly correlated to the orientation of the particle expressed in polar coordinates $\boldsymbol{n} = \cos(\phi)\boldsymbol{e}_r + \sin(\phi)\boldsymbol{e}_\theta$ [Figs. 3(e) and 3(k)]. In the climbing state, $\boldsymbol{n}$ fluctuates around the radial orientation $\boldsymbol{e}_r$. In the orbiting case, there is a finite angle between $\boldsymbol{n}$ and $\boldsymbol{v}$: $\boldsymbol{v} \| \boldsymbol{e}_\theta$ and $\boldsymbol{n}$ is always pointing outwards because of the finite relaxation time τ_n. Finally, one can characterize the angular dynamics with the mean square angular displacement (MSAD) $\langle \Delta\theta(t)^2 \rangle$ with $\Delta\theta(t) = \theta(t) - \theta(0)$ [Figs. 3(f) and 3(l)]. Not surprisingly, in both cases, the MSAD is ballistic at short time and crosses over to a diffusive behavior at long time. More interesting is the dependence on the angular noise: for the climbing dynamics, the noise amplitude affects the magnitude of the velocity and thus of the MSAD, leaving the crossover time unchanged; for the orbiting dynamics, increasing the noise enhances the rate of inversion of the rotation direction and thus reduces the crossover time, thereby reducing the long-time diffusion coefficient.

To rationalize these behaviors, we first study Eqs. (3) and (4) without noise ($D = 0$). In polar coordinates, they read $\dot{r} = v_r$ and

$$\tau_v \left(\dot{v}_r - \frac{v_\theta^2}{r} \right) = \cos(\phi) - v_r - r, \tag{5}$$

$$\tau_v \left(\dot{v}_\theta + \frac{v_r v_\theta}{r} \right) = \sin(\phi) - v_\theta, \tag{6}$$

$$\tau_n \left(\dot{\phi} + \frac{v_\theta}{r} \right) = \cos(\phi) v_\theta - \sin(\phi) v_r. \tag{7}$$

We look for stationary solutions, where $v_r = 0$, $\dot{v}_\theta = 0$, and $\dot{\phi} = 0$, leading to

$$\frac{\tau_v v_\theta^2}{r} = r - \cos(\phi), \tag{8}$$

$$v_\theta = \sin(\phi), \tag{9}$$

$$\frac{\tau_n v_\theta}{r} = \cos(\phi) v_\theta. \tag{10}$$

A trivial solution is $r = 1$, $v_\theta = 0$, $\phi = 0$, which corresponds to the climbing state. When $v_\theta \neq 0$, Eq. (10) simplifies and Eqs. (8)–(10) combine into a closed equation for ϕ; introducing $u = \cos(\phi)^2$, it reads

$$u^2 - \left(1 + \frac{\tau_n}{\tau_v} \right) u + \frac{\tau_n^2}{\tau_v} = 0. \tag{11}$$

This equation has a solution $u \in [0, 1]$, which describes the orbiting state, only if

$$\tau_n \leq \tau_n^* = \begin{cases} 1 & \text{if } \tau_v \leq 1 \\ \frac{\tau_v}{2\sqrt{\tau_v - 1}} & \text{if } \tau_v \geq 1. \end{cases} \tag{12}$$

Finally, linearizing Eqs. (5)–(7) around the stationary solutions, we find that the climbing solution is linearly stable for $\tau_n \geq 1$, and the orbiting solution is linearly stable where it exists [14]. The resulting deterministic phase diagram is shown in Fig. 4(a). The transition from climbing

to orbiting is mainly controlled by τ_n. For $\tau_v < 1$, the transition is continuous. For $\tau_v > 1$, it is discontinuous and both solutions coexist in the region $\tau_v \geq 1$, $1 \leq \tau_n \leq \tau_n^*$. This is illustrated by the evolution of $|v_\theta|$ with τ_n, shown in Figs. 4(b) and 4(d) for $\tau_v = 0.2$ and $\tau_v = 5$. Here the steady solutions were obtained starting with two different initial conditions: one close to the climbing solution, $\boldsymbol{r}_0 = (1, 0)$, $\boldsymbol{v}_0 = (1, 0)$, and $\phi_0 = 10^{-4}$ (IC_1); the other close to the orbiting solution, $\boldsymbol{r}_0 = (1, 0)$, $\boldsymbol{v}_0 = (0, 1)$, and $\phi_0 = 1.6$ (IC_2). The evolution of the distribution of azimuthal velocity through the transition [Figs. 5(c) and 5(e)] also reflects its continuous or discontinuous character: for $\tau_v = 0.2$, the most probable value of v_θ decays continuously to zero as τ_n is increased, whereas it jumps abruptly for $\tau_v = 5$.

For large noise, the probability density recovers a Gaussian shape centered on the center of the parabola [9,12]. At low noise, the fluctuations $X = (\delta r, v_r, \delta v_\theta, \delta\phi)$ around the stationary solutions follow $\dot{X} = -AX + \Xi$, where A is a matrix, whose eigenvalues have a negative real part in a stable state, and Ξ is the Gaussian noise vector associated to ξ [14]. Hence, $X(t)$ is Gaussian and can be characterized completely, giving access to the distributions of the position or the azimuthal velocity [Figs. 3(b), 3(d), 3(h), 3(j), 4(c) and 4(e)] and to the azimuthal velocity-orientation correlations [Figs. 3(e) and 3(k)] [14]. Notably, in the climbing state, the radius r and radial velocity v_r decouple from the azimuthal velocity v_θ and orientation ϕ, which are subject to the angular noise, explaining the very small fluctuations of the radius [Figs. 3(a) and 3(b)]. In the climbing state, we have access to the two regimes of the MSAD through the temporal correlations of the azimuthal velocity, $\langle v_\theta(0)v_\theta(t)\rangle$ [Fig. 3(f)]. The correlations are proportional to D and the crossover from the ballistic to the diffusive regime does not depend on the noise amplitude. Interestingly, for large enough τ_n and τ_v, the eigenvalues of the matrix A are complex, leading to oscillations in the velocity correlation [Fig. 5(a)], which translate into a nontrivial ballistic-diffusive crossover of the MSAD [Fig. 5(c)]. We could check that such oscillations are present in the experimental data [see Fig. 5(b)], showing that inertia matters in the experiments. In the orbiting state, the inversion of the rotation direction is not perturbative and the rate of inversion cannot be computed using this approach. We, however, capture the ballistic part of the MSAD [Fig. 3(l)].

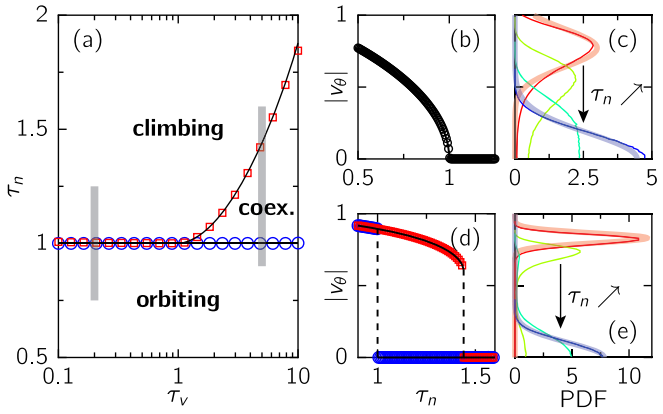

FIG. 4. Noiseless steady states. (a) Phase diagram [the thick gray lines indicate the values of the parameters (τ_v, τ_n) used in the right-hand panels]. (b), (d) Azimuthal velocity as a function of τ_n for $\tau_v = 0.2$ (b) and $\tau_v = 5$ (d), where the symbols represent the steady state obtained from two different initial conditions IC_1 (blue circles) and IC_2 (red squares) as defined in the text. (c e) Distribution of azimuthal velocity through the orbiting (red) to climbing (blue) transition for $D = 0.01$ for $\tau_v = 0.2$ and $\tau_n \in \{0.5, 0.75, 1, 1.25\}$ (b) and $\tau_v = 5$ and $\tau_n \in \{1.2, 1.35, 1.4, 1.6\}$ (d) from simulations (thin lines) and small noise calculation (thick lines).

Altogether using a model of self-propelled particles, previously used to describe active walkers, we have recovered our main experimental observation, namely that a hexbug running in a parabola exhibits two very different dynamical regimes, an orbiting one and a climbing one. Furthermore, we understand why the hexbug transits from the orbiting to the climbing regime when the battery gets low: when F_0 decreases, τ_n increases, while τ_v does not change, hence the observed transition. The fact that intermittent dynamics between the two regimes were observed experimentally is also consistent with the existence of the coexistence region for large enough inertia. Finally, the model is able to predict nontrivial temporal correlations, which are observed experimentally.

Let us conclude with a few remarks. (i) We tested alternative models including self-alignment, but none of them reproduces the observed phenomenology [14]; our experiment puts strong constraints on the equations of motion. (ii) The dynamics described here is in sharp contrast with that of ABP, for which only climbing dynamics exists. This is not because ABP dynamics is overdamped: in the limit $\tau_v \to 0$, Eq. (3) becomes

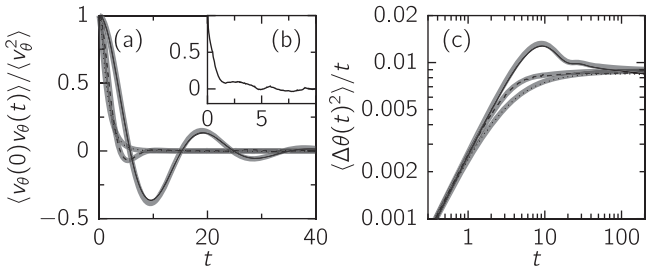

FIG. 5. Time-dependent correlations in the climbing state. (a) Temporal correlations of the azimuthal velocity, and (c) MSAD, for $\tau_n = 2.5$, $D = 0.01$, and $\tau_v = 0.2$, 1, and 5 (dotted, dashed, and solid lines, respectively) in the simulations; thick gray lines show the corresponding weak noise calculation. (b) Experimental correlations of the azimuthal velocity in the climbing state [Figs. 2(a)–2(c)].

$\boldsymbol{v} = \boldsymbol{n} - \boldsymbol{r}$, which is the equation for the velocity of ABP, and the resulting equation for the orientation is

$$\tau_n \dot{\boldsymbol{n}} = -(\boldsymbol{n} \times \boldsymbol{r}) \times \boldsymbol{n} + \sqrt{2D}\xi \boldsymbol{n}_\perp. \tag{13}$$

The climbing to orbiting transition still exists: the particle rotates for $\tau_n < \tau_n^* = 1$ and the azimuthal velocity is $|v_\theta| = \sqrt{1-\tau_n}$. It is thus truly the self-aligning property of $\boldsymbol{n}$ towards $\boldsymbol{v}$ that is responsible for the presence of the two dynamical regimes. (iii) Replacing the harmonic trap with a hard wall of radius R_w (in dimensionless units), an orbiting solution still exists if $\tau_n < R_w$, which slides along the wall at a velocity $v_\parallel = \sqrt{1-(\tau_n/R_w)^2}$ [14]. (iv) The orbiting solution exists, however small the stiffness of the harmonic potential κ provided that the rotational diffusion coefficient $D/\tau_n^2 = \alpha\gamma/(\tau^2\kappa)$ remains small enough.

Finally, let us stress that self-alignment is not limited to macroscopic objects and takes place as soon as the drag force induces a torque when the directions of velocity and self-propulsion are misaligned. This happens *in principle* whenever the design of the active particle includes an embedded orientation $\boldsymbol{n}$: the self-aligning torque arises because the particle, which is by design left-right symmetric with respect to the direction of self-propulsion, is then not always left-right symmetric with respect to the direction of motion. This is easy to imagine for a non-spherical colloid, but it can also arise from differential coating. This is a matter of importance, since it is known that such a coupling is prone to induce collective motion [20]. The present study offers a way to assess self-alignment in a number of active systems, not only those using self-propelled particles similar to the present hexbugs [8,21], but also those in the colloidal realm, using, for instance, acoustic traps [6] or hard wall circular confinement.

[1] C. Bechinger, R. Di Leonardo, H. Löwen, C. Reichhardt, G. Volpe, and G. Volpe, Active particles in complex and crowded environments, Rev. Mod. Phys. **88**, 045006 (2016).

[2] Y. Fily, A. Baskaran, and M. F. Hagan, Dynamics of self-propelled particles under strong confinement, Soft Matter **10**, 5609 (2014).

[3] W. Yan and J. F. Brady, The force on a boundary in active matter, J. Fluid Mech. **785**, R1 (2015).

[4] A. P. Solon, J. Stenhammar, R. Wittkowski, and M. Kardar, Pressure and Phase Equilibria in Interacting Active Brownian Spheres, Phys. Rev. Lett. **114**, 198301 (2015).

[5] N. Nikola, A. P. Solon, Y. Kafri, M. Kardar, J. Tailleur, and R. Voituriez, Active Particles with Soft and Curved Walls: Equation of State, Ratchets, and Instabilities, Phys. Rev. Lett. **117**, 098001 (2016).

[6] R. De Dier, J. Vermant, J. F. Brady, and S. C. Takatori, Acoustic trapping of active matter, Nat. Commun. **7**, 1 (2016).

[7] G. Junot, G. Briand, R. Ledesma-Alonso, and O. Dauchot, Active versus Passive Hard Disks against a Membrane: Mechanical Pressure and Instability, Phys. Rev. Lett. **119**, 028002 (2017).

[8] A. Deblais, T. Barois, T. Guérin, P. H. Delville, R. Vaudaine, J. S. Lintuvuori, J. F. Boudet, J. C. Baret, and H. Kellay, Boundaries Control Collective Dynamics of Inertial Self-Propelled Robots, Phys. Rev. Lett. **120**, 188002 (2018).

[9] A. P. Solon, M. E. Cates, and J. Tailleur, Active Brownian particles and run-and-tumble particles: A comparative study, Eur. Phys. J. Spec. Top. **224**, 1231 (2015).

[10] É. Fodor and M. C. Marchetti, The statistical physics of active matter: From self-catalytic colloids to living cells, Physica (Amsterdam) **504A**, 106 (2018).

[11] C. Maggi, U. M. B. Marconi, N. Gnan, and R. Di Leonardo, Multidimensional stationary probability distribution for interacting active particles, Sci. Rep. **5**, 10742 (2015).

[12] U. Basu, S. N. Majumdar, A. Rosso, and G. Schehr, Active Brownian motion in two dimensions, Phys. Rev. E **98**, 062121 (2018).

[13] Hexbug is a toy automat brand developed and distributed by innovation first, https://www.hexbug.com/.

[14] See Supplemental Material at http://link.aps.org/supplemental/10.1103/PhysRevLett.122.068002 for detailed calculations.

[15] C. Scholz, S. Jahanshahi, A. Ldov, and H. Löwen, Inertial delay of self-propelled particles, Nat. Commun. **9**, 5156 (2018).

[16] C. A. Weber, T. Hanke, J. Deseigne, S. Léonard, O. Dauchot, E. Frey, and H. Chaté, Long-Range Ordering of Vibrated Polar Disks, Phys. Rev. Lett. **110**, 208001 (2013).

[17] S. L. Bore, M. Schindler, K.-D. Nguyen Thu Lam, É. M. Bertin, and O. Dauchot, Coupling spin to velocity: Collective motion of Hamiltonian polar particles, J. Stat. Mech. (2016) 033305.

[18] K.-D. Nguyen Thu Lam, M. Schindler, and O. Dauchot, Self-propelled hard disks: Implicit alignment and transition to collective motion, New J. Phys. **17**, 113056 (2015).

[19] See https://www.hexbug.com/nano.

[20] K.-D. Nguyen Thu Lam, M. Schindler, and O. Dauchot, Self-propelled hard disks: Implicit alignment and transition to collective motion, New J. Phys. **17**, 113056 (2015).

[21] L. Giomi, N. Hawley-Weld, and L. Mahadevan, Swarming, swirling and stasis in sequestered bristle-bots, Proc. R. Soc. A **469**, 20120637 (2013).